

Article

# Hierarchical Symmetry-Breaking Model for Stem Cell Differentiation

Nikolaos K. Voulgarakis 

Department of Mathematics and Statistics, Washington State University, Pullman, WA 99164, USA; n.voulgarakis@wsu.edu

**Abstract:** Waddington envisioned stem cell differentiation as a marble rolling down a hill, passing through hierarchically branched valleys representing the cell's temporal state. The terminal valleys at the bottom of the hill indicate the possible committed cells of the multicellular organism. Although originally proposed as a metaphor, Waddington's hypothesis establishes the fundamental principles for characterizing the differentiation process as a dynamic system: the generated equilibrium points must exhibit hierarchical branching, robustness to perturbations (homeorhesis), and produce the appropriate number of cells for each cell type. This article aims to capture these characteristics using a mathematical model based on two fundamental hypotheses. First, it is assumed that the gene regulatory network consists of hierarchically coupled subnetworks of genes (modules), each modeled as a dynamical system exhibiting supercritical pitchfork or cusp bifurcation. Second, the gene modules are spatiotemporally regulated by feedback mechanisms originating from epigenetic factors. Analytical and numerical results show that the proposed model exhibits self-organized multistability with hierarchical branching. Moreover, these branches of equilibrium points are robust to perturbations, and the number of different cells produced can be determined by the system parameters.

**Keywords:** cell differentiation; pitchfork bifurcations; cusp bifurcation; symmetry breaking; self-organized multistability; normal forms; bifurcation theory

**MSC:** 92-10



**Citation:** Voulgarakis, N.K.

Hierarchical Symmetry-Breaking Model for Stem Cell Differentiation. *Mathematics* **2024**, *12*, 1380. <https://doi.org/10.3390/math12091380>

Academic Editor: Takashi Suzuki

Received: 3 April 2024

Revised: 25 April 2024

Accepted: 30 April 2024

Published: 1 May 2024



**Copyright:** © 2024 by the author. Licensee MDPI, Basel, Switzerland. This article is an open access article distributed under the terms and conditions of the Creative Commons Attribution (CC BY) license (<https://creativecommons.org/licenses/by/4.0/>).

## 1. Introduction

Early stages of embryonic development depend on the ability of pluripotent stem cells to proliferate and differentiate into different types of specialized cells that are essential for the formation of multicellular organisms. As shown in Figure 1a, pluripotent stem cells first become multipotent progenitors, which then differentiate further into various cell types within their specific lineages; while this process may appear complex and delicate at the cellular level [1,2], it is remarkably robust when observed at the macroscopic level.

In an attempt to elucidate the fundamental aspects of stem cell differentiation, Waddington introduced a visual analogy captured in the now-iconic sketch from their 1957 work [3] (see, Figure 1b). In this analogy, the pluripotent stem cell is represented by a marble resting at the peak of a hill. The differentiation begins as the marble rolls downhill, passing through various valleys, each corresponding to different cell states, such as progenitors or subsequent progenitors. The terminal valleys at the base of the hill represent specialized cells. Although this graph is just a metaphor for the actual process, it elegantly depicts three essential aspects of stem cell differentiation [4,5]. First and foremost, differentiation can be described as a hierarchically branched process. This means that at each stage of differentiation, a cell must be capable of choosing among various potential future states within its lineage. This decision-making (branching) process continues until the final decision point, leading to the formation of specialized cells. Cell differentiation

progresses forward in time, with rare exceptions where cells can return to a previous branching point. The second crucial characteristic is homeorhesis, i.e., the ability of cells to maintain their dynamics at each branch even in the presence of moderate noise. Third, the overall differentiation process must exhibit robustness, consistently generating the precise number of cells required for the development of the multicellular organism.

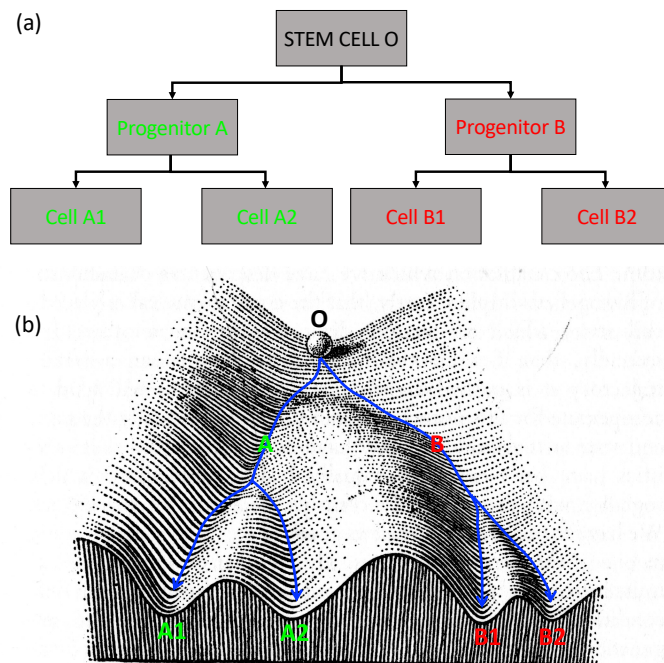


**Figure 1.** (a) Schematic representation of the pluripotent stem cell (O) differentiation into multipotent progenitors (A and B) and subsequently into terminally differentiated cells (A1, A2, B1, B2). (b) Waddington's epigenetic landscape (adapted from [3]).

It has been suggested that the branching points in Waddington's epigenetic landscape can be thought of as symmetry-breaking events [4,6–8]. According to this hypothesis, stem cells are in a highly symmetric cell state because they can express multiple genes that are specific to their progenitors, while progenitor cells are less symmetric because they only express a subset of these genes that are specific to their lineage. Specialized cells have the lowest possible symmetry because they can only express genes that are related to their own functions. In this simplified picture, we can see two symmetry-breaking events. First, the highly symmetric stem cells differentiate into less symmetric progenitor cells, and second, the progenitor cells differentiate into specialized cells with the lowest possible symmetry. Symmetry-breaking events can occur at either the cellular or population level [6,9–15]. Researchers have explored both scenarios through theoretical and experimental studies. It is likely that symmetry breaking may occur at both levels.

Mathematically, stem cell differentiation is often modeled by systems of differential equations, where the variables represent gene expression levels [16,17]. The gene expression is regulated by Hill's functions, which capture the complex nature of the gene regulatory network (GRN). The process of gene suppression is usually represented by simple, typically linear, dissipative terms. With appropriate parameter adjustments, the system can be driven through bifurcation points (pitchfork or saddle-node) that lead to the emergence of new stable solutions. The connection of the bifurcation diagram with the differentiation process is straightforward: (a) a single stable branch represents the stem cell state, (b) the bifurcation point indicates the decision-making (symmetry-breaking) event, and (c) the new stable solutions represent the gene expression levels of the differentiated cells. In cases where the GRN includes a large number of genes, the bifurcation diagram becomes increasingly difficult to comprehend and analyze. To overcome this limitation, several recent

theoretical works make use of the normal forms of supercritical pitchfork and saddle-node bifurcation [18–22]. Normal forms represent the simplest possible mathematical model, with the fewest parameters that exhibit these bifurcations. The resulting state variables of the normal forms are not straightforwardly connected to the gene expression levels. Their relationship may be highly nonlinear and difficult to predict in general [21]. Despite lacking detailed information on realistic biochemical networks, models based on normal forms can still make experimentally testable, quantitative predictions about the produced cells' ratio [22].

The systems of differential equations based on detailed biochemical networks or normal forms face a couple of challenges. First, they do not generally describe a large number of branching events (multistability), and second, the symmetry-breaking events do not self-organize spontaneously as in stem cell differentiation. The latter was recently addressed in one of our publications, where stem cells were modeled as a dynamical system exhibiting supercritical or saddle-node bifurcation [8]. By introducing a feedback mechanism that controls the transcriptional noise, we demonstrated that the cell can autonomously navigate through various bifurcation points and spontaneously differentiate into a number of stationary or dynamic attractors (limit cycles). Reference [8] also showed the possibility of describing the first branching point at the top of Waddington's epigenetic landscape.

The aim of this paper is to generalize [8] in order to model self-organized multistability that captures the main characteristics of Waddington's epigenetic landscape. This generalization is inspired by two important works [4,5]. First, the authors of [4] hypothesized that a GRN consists of a collection of hierarchically coupled subnetworks of genes (modules). Each module was described by a dynamical system that exhibits a tristability. One stable node represents the undifferentiated state of the module, while the other two represent two different possible functions. Initially, all modules are in the undifferentiated state. The presence of noise causes spontaneous symmetry breaking in the first module, leading it to assume one of two possible functions. Then, this decision triggers the subsequent modules to go through their own bifurcation point. This transition was controlled by modulating the undecided module parameters through a piece-wise function with respect to the state of the first module. In the end, all modules have gone through their own bifurcation point and have assumed a specific stable state. All these states collectively determine the function of the differentiated cell. Second, Matsushita and Kaneko also presented a dynamical system that is capable of describing the basic features of Waddington's epigenetic landscape [5]. In their work, each gene of the GRN was modeled by a differential equation that assumes an "on" or "off" stable state. Furthermore, the authors assumed that each gene is regulated by auxiliary variables, also described by differential equations, that represent epigenetic modifications. Collectively, the system showed hierarchical branching, robustness, and a unique cell ratio of differentiated cells. The advantage of this approach is that it provides a more comprehensive understanding of how the GRN can self-regulate and achieve a stable state in the presence of perturbations.

This work here presents an autonomous dynamical system that can describe the three fundamental aspects of the epigenetic landscape. The model is based on the concept of (a) GRN modularity [4] and (b) parameter regulation due to epigenetic factors [5,8]. Specifically, this work assumes that the GRN consists of a number of hierarchically interacting subnetworks (modules). These modules are capable of determining their own function. For simplicity, we assume that these functions are represented by the fixed points of a supercritical pitchfork or cusp bifurcations. These modules are then coupled together with feedback mechanisms controlled by intrinsic and extrinsic factors (i.e., cell–cell interaction or epigenetic factors). By introducing a spatiotemporal hierarchy, it is possible to construct trajectories that depict the dynamics of the marble in the epigenetic landscape. Overall, the proposed model has the potential to describe the three basic properties of Waddington's landscape: hierarchical branching, homeorhesis, and conservation of the differentiated cells ratio. Moreover, by appropriately tuning the parameters, the epigenetic landscape can include cellular states that are highly improbable. This is interesting because it has been proposed that cancer cell states correspond

to these unlikely states in the epigenetic landscape [23]. Finally, the work presented here can serve as a model for direct or indirect reprogramming, also known as transdifferentiation and dedifferentiation, respectively [6,24–26].

The paper's organization is straightforward. The following section presents the mathematical model. Specifically, Section 2.1 briefly discusses previous work [8], while Section 2.2 introduces its extension. Section 3 presents theoretical and numerical analysis of the proposed model and discusses its capability of modeling certain aspects of Waddington's epigenetic landscape. Finally, Section 4 summarizes this paper.

## 2. Mathematical Model

This study employs the normal forms of supercritical pitchfork and cusp bifurcation to simplify the complex behavior of GRNs. Although these models are not as detailed as traditional biochemical models [16], they are still capable of describing the phenomenology of decision-making events depicted in the Waddington epigenetic landscape.

In this section, standard linear stability analysis is used to study the dynamic behavior of the proposed dynamical system. Representative simulations also complement this analysis to demonstrate spontaneous symmetry-breaking events and cell fate decisions. Fluctuations due to finite-size effects and gene expression noise [1,2] were represented by adding white noise terms to the stem-cell state Equation (see, for example, [8]). Mathematically, such terms are expressed as  $\sigma dW_t$ , where  $\sigma$  is the variance of white noise, and  $dW_t$  represents independent Wiener increments. The numerical solution of the dynamical systems was obtained using the standard Euler–Maruyama method, with an integration step of  $dt = 10^{-3}$ . In all simulations, the variance has been constant at  $\sigma = 0.2$ . The Waddington's epigenetic landscape was constructed using the concept of quasi-potential [27],

$$\Phi(m, t) \propto -\log[P(m, t)], \quad (1)$$

where  $P(m, t)$  is the probability of finding the system at state  $m$  at time  $t$ . The probability is computed over  $10^5$  independent stochastic trajectories  $m(t)$ . Note that this approach cannot fully reconstruct the potential landscape due to the rare occurrence of some stable solutions. These states will be referred to as silenced states within a fixed number of independent simulations. In this work, they correspond to cells that rarely express specific genes, which are termed gene silencing [28].

### 2.1. Spontaneous Symmetry Breaking Model

In our latest publication [8], we presented a model that describes the process of a stem cell differentiating into two progenitor cells. This model is based on a standard pitchfork bifurcation coupled with a feedback mechanism that regulates transcriptional noise. The mathematical expression of this model is

$$\frac{dm}{dt} = rm - m^3 \quad (2)$$

$$\frac{dr}{dt} = G(M^2 - m^2). \quad (3)$$

Let us first analyze Equation (2), which is the normal form of the supercritical pitchfork bifurcation. Here,  $m$  represents the stem cell state. Specifically,  $m = 0$  corresponds to pluripotent stem cells, while  $m \neq 0$  describes differentiated cells. The parameter  $r$  controls the bifurcation diagram. For  $r \leq 0$ , the pluripotent stem cell state is the only stable solution. For  $r > 0$ , the stem cell state becomes unstable, and two symmetric stable states  $m = \pm\sqrt{r}$  emerge that represent the differentiated cells. Thus, we can only have a stem cell state ( $m = 0$ ) if  $r \leq 0$ . In self-organized systems or processes, such as stem cell differentiation, control parameters become dynamic variables that are regulated by external stimuli and internal dissipation. One way to incorporate this mechanism into Equation (2) is to assume that epigenetic factors increase the control parameter at a constant rate  $B$ , while internal

mechanisms decrease it through a state-dependent dissipating term  $Gm^2$ , where  $G$  is the dissipation (relaxation) constant (see, for example, [29]). Thus, the differential equation governing the dynamics of the control parameter could be expressed as  $\dot{r} = B - Gm^2$ . To simplify this equation, one can factor  $G$  and define  $M^2 = B/G$ , resulting in Equation (3). The choice of the quadratic term  $m^2$  instead of the linear  $m$  is to maintain the  $m \rightarrow -m$  invariance of the pitchfork bifurcation.

In [8], the variable  $r$  was defined as  $r = 1 - \zeta$ , where  $\zeta$  represented the level of transcriptional noise. Here,  $r$  is generalized as any variable that regulates the spontaneous decision-making events in stem cell differentiation. This new definition of  $r$  can be associated with parameters such as the transcriptional rate and critical concentration of proteins that are used in more detailed dynamical systems of stem cell differentiation.

The dynamical system of Equations (2) and (3) exhibits two symmetric asymptotically stable equilibrium states [8]

$$(m^*, r^*) = (\pm M, M^2). \tag{4}$$

For  $G > M^2/2$ ,  $G = M^2/2$ , or  $G < M^2/2$ , the equilibrium solutions are stable spirals, degenerate nodes, or stable nodes, respectively. Thus, any initial stem cell state ( $m \approx 0$  and  $r < 0$ ) will eventually differentiate into either of the  $\pm M$  cell types with equal probability. This can be seen in Figure 2a, where several representative trajectories of stem cell differentiation are demonstrated. All of these trajectories begin from the stem cell state ( $m(0) = 0$  and  $r(0) = -5$ ) and eventually reach a critical point where a spontaneous decision is made, leading to either the  $+M$  or  $-M$  cell state. This decision is made randomly due to the presence of white noise in the system. Once the trajectory has well passed the bifurcation point, it remains within the chosen branch of equilibrium solutions. After passing the bifurcation point, none of the  $10^5$  simulated trajectories changed branches. To demonstrate this result, several trajectories are embedded in the density plot of the quasi-potential  $\Phi(m, t)$ . In Figure 2b, we can see the three-dimensional (3D) quasi-potential, which is qualitatively consistent with the first differentiation in the Waddington epigenetic landscape. However, it is too symmetric to be realistic (refer to Figure 1b). Here, it is essential to note that the value of parameter  $G$  determines the speed of spontaneous symmetry breaking. Higher  $G$  values result in faster differentiation. Hence,  $G^{-1}$  can be considered the time it takes for differentiation to occur.

To create a more realistic epigenetic landscape, this study takes into account an external field,  $\mu$ , which also originates from epigenetic factors. This external field introduces an asymmetry in the potential function of the system and promotes the differentiation of specific cell types. The method described below allows for the adjustment of the ratio between two distinct cell types produced during symmetry breaking. This is considered one of the three most important properties of cell differentiation. Specifically, Equations (2) and (3), are modified as follows:

$$\frac{dm}{dt} = rm - m^3 - \mu, \tag{5}$$

$$\frac{dr}{dt} = G(M^2 - m^2). \tag{6}$$

The first equation represents the normal form of the cusp bifurcation [30]. It should be noted that this model exhibits bistability accompanied by a hysteresis loop. The second equation is the same standard feedback mechanism that was used in [8]. This modified dynamical system has two equilibrium states

$$(m^*, r^*) = (\pm M, M^2 \pm \frac{\mu}{M}) = E_{\pm}. \tag{7}$$

Linear stability analysis trivially shows that  $E_-$  is always stable, while  $E_+$  is stable for  $\mu < 2M^3$ , center for  $\mu = 2M^3$ , and unstable for  $\mu > 2M^3$ . For  $\mu > 2M^3$ , all initial conditions different from  $E_+$  will asymptotically approach  $E_-$ . In this case, one can say that the cell  $E_+$  has been eliminated from the epigenetic landscape. This guarantees that the system, starting from the pluripotent stem cell state ( $m(0) = 0$  and  $r(0) < 0$ ), will

always differentiate to either  $+M$  or  $-M$ . In other words, the differentiation process is guaranteed. Note that by tuning the value of  $\mu$ , the potential energy of the supercritical pitchfork bifurcation is tilted. This process creates an imbalance in the system that favors certain cell states. In particular, when  $\mu > 0$ , there is a greater chance of producing the cell  $-M$ , whereas if  $\mu < 0$ , the stem cell is more likely to differentiate into the  $+M$  cell. This is demonstrated in Figure 2c, where multiple cell state trajectories are presented for  $\mu = 0.75$ . The system always begins from  $m = 0$  and  $r = -5$  representing the pluripotent state. Since  $\mu > 0$ , differentiation into cell  $-M$  is more likely than cell  $+M$ . This is also apparent in Figure 2d, which displays the 3D quasi-potential. The potential well associated with cell  $-M$  is deeper than that of cell  $+M$ . In Figure 2e,f,  $\mu$  is increased further to  $\mu = 1.5$ , causing the well located at  $+M$  to disappear. If  $\mu < 0$ , cell state  $+M$  would have been promoted instead. Thus, this model can create an imbalance in the epigenetic potential that favors one cell over another, and in some cases, certain cell types can even be silenced within the limited number of independent simulations.

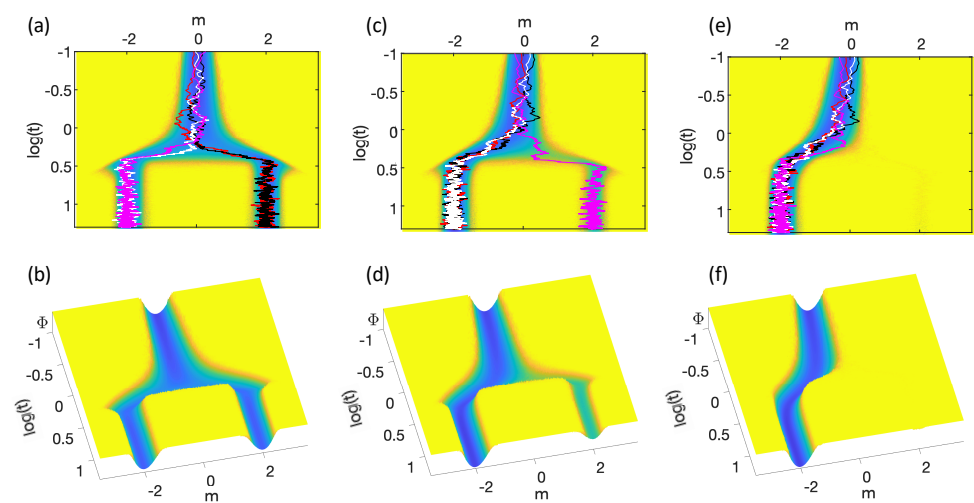


**Figure 2.** First row shows representative trajectories of a single module embedded on the density plot of the quasi-potential function. The second row shows the 3D representation of the quasi-potential versus  $m$  and time. In (a,b),  $\mu = 0$ . In (c,d),  $\mu = 0.75$ . In (e,f),  $\mu = 1.5$ . In all subfigures,  $M = 2$  and  $G = 1$ . The quasi-potentials were constructed using Equation (1) with  $10^5$  independent trajectories. Blue and yellow colors correspond to low and high values of the quasi-potential, respectively.

## 2.2. GRN Modularity

It is evident that many biological systems, including GRN, display modularity [31–35]. In simple terms, those systems consist of weakly interconnected modules that carry out specific tasks or respond to particular stimuli. It has been suggested that modularity is advantageous as it enables efficient information processing and allows for the integration of diverse inputs and outputs to coordinate complex biological functions. In [4], the authors suggested that GRN also exhibits a hierarchical modularity during differentiation. The differentiation process begins when a sub-network of genes (module) first undergoes symmetry breaking, causing the module to perform a specific function in the cell. This function then triggers a symmetry breaking in the second module in the hierarchy, and so on and so forth. Collectively, the behavior of all modules together determines the type of the cell.

Mathematically, this idea was formulated by assuming that each module is represented by a dynamical system exhibiting tristability. At the beginning of the differentiation process, the first dynamical system in the hierarchy passes through the bifurcation point and spontaneously selects a specific stable solution that represents a particular function. This stable solution then triggers a spontaneous symmetry breaking in the subsequent dynamical systems. The authors were able to show that this approach reproduces the hierarchical

branching, and the produced branches of equilibrium points are stable to internal noise. Although the control of the produced ratio of cells was discussed in the paper, it was not extensively covered. The work presented here builds upon [4] and attempts to offer a more systematic approach to constructing the Waddington epigenetic landscape.

More specifically, this section considers that the GRN consists of a number of weakly coupled gene modules. A schematic representation of a cell with three of these modules is shown in Figure 3a. Each module starts in a neutral state but eventually undergoes a symmetry-breaking event that assigns a specific role or function for the cell. This symmetry-breaking occurs in a hierarchical manner and can be mathematically described by the models presented in Section 2.1. Assuming that the state of each module is denoted by  $m_i$ , where  $i = 1, 2, 3$ , at  $t = 0$ , all modules are in the undifferentiated state “0,0,0”, i.e., all  $m_i = 0$  (Figure 3b). External factors trigger the first decision-making event, causing the first module to assume the “+” state at time  $t_1$  (Figure 3c). The current cell state “+,0,0” may represent a common progenitor cell. This state triggers the symmetry-breaking event in the second module, and it takes on the “-” state at time  $t_2$  (Figure 3d). The state “+,-,0” may represent a more specific progenitor, such as a myoepithelial progenitor. Finally, at time  $t_3$ , the third decision-making event is triggered by the current state of the cell, and the third module assumes the “+” state (Figure 3e). At this point, the entire cell is characterized by a “+,-,+” state, which corresponds to a terminally differentiated cell. As demonstrated below, even if we assume a weak coupling between gene modules, the cell can undergo differentiation.

To mathematically formulate the schematic diagram shown in Figure 3, it is assumed that the GRN consists of  $n$  hierarchically coupled gene modules. Each module is described by a self-regulated dynamical system discussed in Section 2.1. Furthermore, we assume that the modules are weakly coupled, and their spontaneous symmetry breaking is triggered in a sequential manner. Let us denote the state of the cell as  $\mathbf{m} = (m_1, \dots, m_n)^T$  and the dynamic parameters as  $\mathbf{r} = (r_1, \dots, r_n)^T$ . Then, the dynamical system describing the cell differentiation is

$$\frac{d\mathbf{X}}{dt} = F(\mathbf{X}; \boldsymbol{\mu}, \mathbf{G}, \mathbf{M}), \tag{8}$$

where  $\mathbf{X} = (\mathbf{m}, \mathbf{r})^T$ ,  $\boldsymbol{\mu} = (\mu_1, \dots, \mu_n)^T$  is the external vector field,  $\mathbf{G} = (G_1, \dots, G_n)^T$  represent the relaxation parameters of each module, and  $\mathbf{M} = (M_1, \dots, M_n)^T$ . The vector field is  $F = (f_1, \dots, f_n, g_1, \dots, g_n)^T$ , where

$$f_i(m_i, r_i; \mu_i) = r_i m_i - m_i^3 - \mu_i \tag{9}$$

$$g_i(m_i; G_i, M_i) = G_i(M_i^2 - m_i^2). \tag{10}$$

To keep the analysis as simple as possible, this work considers a simple spatial hierarchical coupling through the parameters  $M_i$  according to the following equation

$$M_i = \begin{cases} \bar{M}_1 + \sum_j d_{1j} m_j & i = 1 \\ \sum_{j < i} c_{ij} m_j + \sum_j d_{ij} m_j & i > 1 \end{cases} \tag{11}$$

where  $\bar{M}_1$  is a parameter decided by external factors. The coefficients  $c_{ij}$  determine the hierarchical coupling and are non-zero only for  $j < i$ . This condition ensures that influence will happen in a hierarchical manner, i.e., the first module affects the second module, then the first and second modules affect the third module, and so on. The matrix  $d_{ij}$  weakly couples different modules simultaneously. As we will see below, the external fields  $\mu_i$  and interaction strengths  $d_{ij}$  offer the necessary asymmetry that makes the system more realistic and tunable.

To project the  $n$ -dimensional state space  $\mathbf{m}$  into a single generic cell-state coordinate, as in Waddington’s epigenetic landscape, one may choose different functions. Here, this coordinate is defined as

$$\mathcal{M} = m_1 + \dots + m_n. \tag{12}$$

The model parameters can be set to arbitrary values as long as the system has stable solutions. However, to achieve a hierarchical branching visually similar to Waddington’s landscape (see Figure 1b), specific parameter values have been selected in Sections 3.1 and 3.2. If parameters are chosen randomly, a more complex, rugged potential landscape is produced. This case is discussed in Section 3.3.

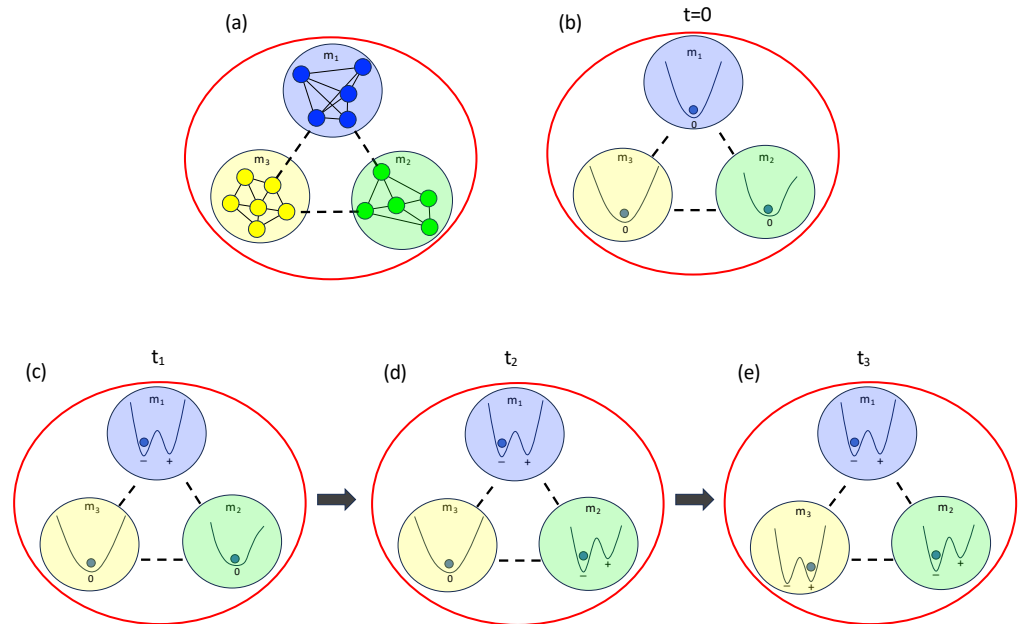


**Figure 3.** (a) Schematic representation of a GRN consisting of three gene modules. Subfigure (b) shows the mathematical representation of each module as a dynamical system exhibiting pitchfork bifurcation. The single wells of all modules at time  $t = 0$  indicate that none of them has gone through a spontaneous symmetry-breaking event yet. Subfigures (c), (d), and (e) show the state of the modules at times  $t_1$ ,  $t_2$ , and time  $t_3$ , respectively, such that  $0 < t_1 < t_2 < t_3$ . Clearly, the modules  $m_1$ ,  $m_2$ , and  $m_3$  experience a hierarchical symmetry breaking. Subfigure (e) illustrates the terminally differentiated cell.

### 3. Results

#### 3.1. Symmetric Hierarchical Branching

##### 3.1.1. Case $n = 2$

Let us first consider a scenario where we have only two modules ( $n = 2$ ). Let us further assume that there is no external field or weak interaction, i.e.,  $\mu_i = 0$  and  $d_{ij} = 0$  for any  $i, j$ . Without loss of generality, we set  $\bar{M}_1 = 7$  and assume that all  $c_{ij}$  values are zero, except for  $c_{2,1} = 0.5$ . This choice of  $c_{ij}$  corresponds to a simple case where the first module affects the second module but not vice versa. The choice of the parameters here facilitated a visually easy to comprehend hierarchical branching.

The equilibrium points of the system (8) with  $M_i$  given in Equation (11) are discussed in Section 2.1 (see Equation (4)):

$$(m_i^*, r_i^*) = (\pm M_i, M_i^2). \tag{13}$$

As always, the system starts from the pluripotent stem cell state, i.e., all  $m_i(0) = 0$  and all  $r_i(0)$  assume negative values, for example,  $r_i(0) = -5$ . Based on Equation (11), only  $M_1 = \bar{M}_1$  is different than zero. Thus, the first module will first achieve the equilibrium points  $m_1^* = \pm M_1$ . Then,  $M_2 = c_{2,1}m_1^*$  becomes nonzero, and the second module will reach the equilibrium point  $m_2^* = \pm M_2$ . Since it is assumed that the two-dimensional state space

is projected onto a generic state coordinate  $\mathcal{M} = m_1 + m_2$ , the system has the following  $2^n = 4$  equilibrium cell states:

$$\mathcal{M}^* = (-M_1 - M_2, -M_1 + M_2, +M_1 - M_2, +M_1 + M_2). \tag{14}$$

The equilibrium points for the dynamic variables are determined by using Equation (13), i.e.,  $r_i^* = (m_i^*)^2$ . Note that  $(m_1^*, r_1^*)$  is asymptotically stable due to the analysis presented in Section 2.1. This implies that due to the simplistic hierarchical coupling used in this section,  $(m_2^*, r_2^*)$  also has the same stability. Thus, all equilibrium cell states in Equation (14) are asymptotically stable. One can more formally prove this stability by computing the  $4 \times 4$  Jacobian of the dynamical system (8) at each equilibrium point and showing that the real part of all of its eigenvalues is negative. The Supplementary Materials includes simple codes that can be used to verify the stability of the dynamical system.

Figure 4a presents the trajectories of  $m_1(t)$ ,  $m_2(t)$ , and the cell state coordinate  $\mathcal{M}(t) = m_1(t) + m_2(t)$ . Note that the trajectory of  $m_1(t)$  experiences a symmetry breaking first (red line) to assume the state  $+M_1$  and  $m_2(t)$  (blue line) follows at a later time to assume the equilibrium state  $-M_2$ . Overall, the cell (black line) entails having the state  $\mathcal{M} = +M_1 - M_2$ . In Figure 4b, we present several trajectories showing that there is no bias in which one of the four cell states in Equation (14) will be picked at the end. These trajectories are embedded in the density plot of the quasi-potential  $\Phi(\mathcal{M}, t)$ . The 3D version of  $\Phi(\mathcal{M}, t)$  is presented in Figure 4c. Once again, simulations revealed that the hierarchical branching of equilibrium solutions is robust to random fluctuations. Although the perfect symmetry of this potential is not realistic, it qualitatively captures Waddington’s epigenetic landscape presented in Figure 1b.

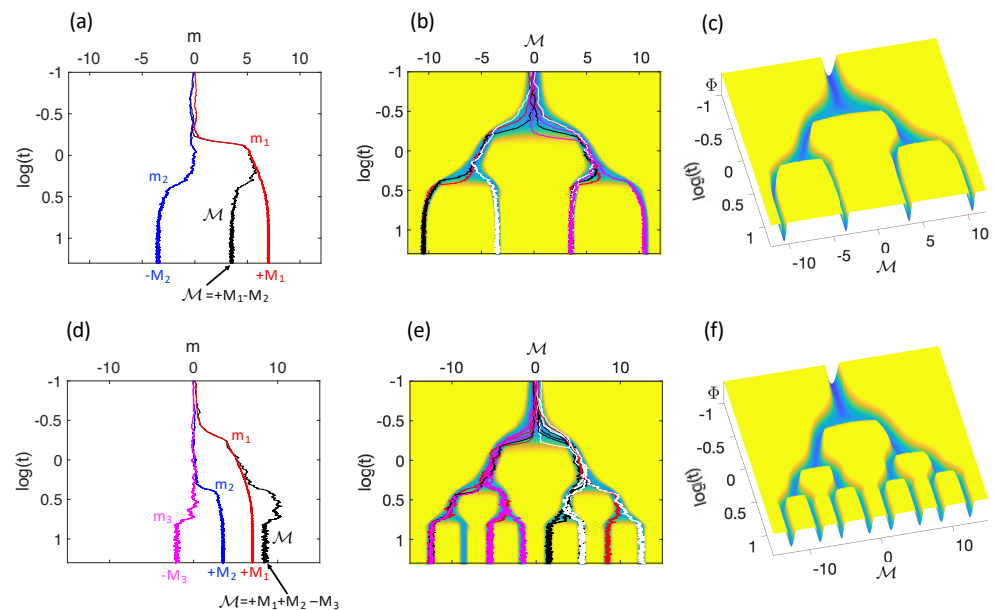


**Figure 4.** The first row shows an example of a cell consisting of two modules ( $n = 2$ ). Specifically, subfigure (a) shows the trajectories of  $m_1$  (red line) and  $m_2$  (blue line), along with the projected generic coordinate  $\mathcal{M} = m_1 + m_2$  (black line). Subfigure (b) shows the density plot of the quasi-potential, along with several representative trajectories. Subfigure (e) shows the 3D version of the quasi-potential. The second row represents an example of a stem cell that consists of three modules ( $n = 3$ ). Subfigures (d), (e), and (f) are equivalent to subfigures (a), (b), and (c), respectively, for the case of  $n = 2$ . The parameters for  $n = 2$  are given in Section 3.1.1 and for  $n = 3$  in Section 3.1.2. In all cases,  $\mu = 0$  and  $d = 0$ . Blue and yellow colors correspond to low and high values of the quasi-potential, respectively.

### 3.1.2. Case $n = 3$

We can apply the previous analysis to any number of modules. To give a clear comparison, let us consider another example with three modules ( $n = 3$ ). All the parameters and conditions remain the same as in the previous case, except that we set  $c_{3,2} = 0.571$ . Consequently, only the first module affects the second module, and similarly, only the second module affects the third one in a sequential manner. The stability analysis shows that the system's equilibrium points for  $m_i$  are  $m_1^* = \pm M_1$ ,  $m_2^* = \pm M_2$ , and  $m_3^* = \pm M_3$ , where  $M_2 = c_{21}m_1^*$  and  $M_3 = c_{32}m_2^*$ . Thus, the generic cell state coordinate  $\mathcal{M}$  has  $2^n = 8$  asymptotically stable equilibrium points:

$$\begin{aligned} \mathcal{M}^* = \{ & -M_1 - M_2 - M_3, -M_1 - M_2 + M_3, -M_1 + M_2 - M_3, -M_1 + M_2 + M_3, \\ & +M_1 - M_2 - M_3, +M_1 - M_2 + M_3, +M_1 + M_2 - M_3, +M_1 + M_2 + M_3 \}. \end{aligned} \quad (15)$$

Similarly to the previous example, Figure 4d demonstrates the time evolution of the three modules  $m_1$ ,  $m_2$ , and  $m_3$ , as well as the cell state coordinate  $\mathcal{M} = m_1 + m_2 + m_3$ . As always, the system starts from the pluripotent stem cell state, i.e.,  $m_i(0) = 0$  and  $r_i(0) = -5$ . Note that the trajectory of  $m_1(t)$  experiences a symmetry breaking first (red line) to assume the state  $+M_1$ , then  $m_2(t)$  (blue line) follows to assume the equilibrium state  $+M_2$ , while  $m_3(t)$  experiences symmetry breaking at a later time to occupy state  $-M_3$ . At that point, the terminal cell state is (black line)  $+M_1 + M_2 - M_3$ . In Figure 4e, we present a number of different cell-state trajectories. Similar to the example with  $n = 2$ , the equilibrium solutions are stable. The 3D quasi-potential,  $\Phi(m, t)$ , is presented in Figure 4f. This graph shows how Waddington's epigenetic landscape presented in Figure 1b could be qualitatively extended to describe a third differentiation level. As in the previous case, all states are equally probable.

### 3.2. Asymmetric Spatial Hierarchical Branching

The previous section helped us gain a better understanding of how Equation (8) can describe hierarchical branching that is robust to random fluctuations. However, due to the simplicity and symmetry of the hierarchical coupling, all different types of differentiated cells are equally probable. Here, we will discuss how the proposed dynamical system can model the differentiation process and produce the necessary number of differentiated cells, which differs for each cell type. This can be achieved by considering non-zero fields  $\mu$  and inter-module interactions  $d$ . This section will only consider a cell with three hierarchically coupled gene modules ( $n = 3$ ). The remaining parameters are identical to those in Section 3.1.2. For comparison reasons, the density plot of Figure 4e is copied in Figure 5a.

We will first consider an example with

$$\mu = (1, -1, 1)^T, \quad (16)$$

and set the interaction matrix  $d = 0$ . The equilibrium points for the three  $m_i$  are also given by Equation (7)

$$(m_i^*, r_i^*) = (\pm M_i, M_i^2 \mp \frac{\mu_i}{M_i}). \quad (17)$$

It can be shown, through a similar analysis as Section 3.1.2, that the equilibrium states of the generic cell-state coordinate remain the same as those in Equation (15). However, the presence of the external field favors specific directions during the spontaneous symmetry-breaking events. This leads to differentiation through pathways that promote certain cell states. An example is shown in the density plot of the quasi-potential presented in Figure 5b. In this plot, we can see that some equilibrium points (differentiated cells) are more probable than others. Additionally, for extremely high values of  $\mu_i$ , some states may be occupied rarely or even disappear. The remarkably low probability can be attributed to mutations, cancerous cell states, or silenced cell states.

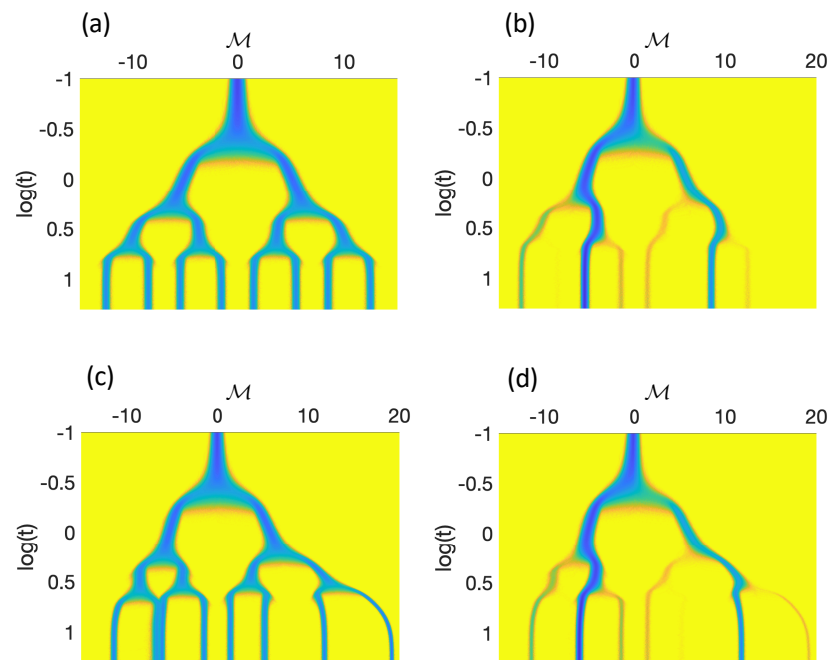


**Figure 5.** Four different density plots of the quasi-potential are presented in this figure. Subfigure (a) is the same as Figure 4e and has been included for comparison purposes. The parameters used in subfigure (a) are the same as in 3.1.2. All parameters remain the same in the rest of the subfigures, except for  $\mu$  and  $d$ . Specifically, in (b),  $\mu$  is given by Equation (16) and  $d = 0$ . In (c),  $\mu = 0$  and  $d$  is given by Equation (18). Finally, in (d),  $\mu$  and  $d$  are given by Equations (16) and (18), respectively. In these plots, blue and yellow colors correspond to low and high values of the quasi-potential, respectively.

A different way to introduce an asymmetry in the system’s state space is to assume a weak inter-module interaction, such as the following:

$$d = \begin{bmatrix} 0.107 & 0.313 & -0.075 \\ -0.009 & 0.056 & 0.135 \\ -0.020 & 0.111 & 0.172 \end{bmatrix}. \tag{18}$$

To better understand the impact of this interaction, we will set  $\mu = 0$ . The equilibrium points  $m_i^*$  can be derived by solving the following system of linear equations:

$$m_1 = \pm (\bar{M}_1 + \sum_j d_{1j}m_j) \tag{19}$$

$$m_{i>1} = \pm (\sum_{j<i} c_{ij}m_j + \sum_j d_{ij}m_j). \tag{20}$$

Then, the corresponding  $r_i^*$  are

$$r_i^* = (m_i^*)^2 + \frac{\mu_i}{m_i^*}. \tag{21}$$

The eight different equilibrium solutions of the generic coordinate  $\mathcal{M}$  are given by Equation (12). Figure 5c demonstrates the density plot of the quasi-potential,  $\Phi(\mathcal{M}, t)$ . It is clear that the interaction matrix  $d$  introduces an asymmetry in the state space, compared to the unperturbed case presented in Figure 5a. This asymmetry causes certain states to merge while others become more distant. It is important to note that the probability of having each cell state remains equal.

To ensure that the system makes physical sense, all equilibrium points  $X^* = (m^*, r^*)^T$  must be asymptotically stable. This can be verified by computing the Jacobian of  $F$  at

each equilibrium point and showing that the real part of all of its eigenvalues is negative. However, this is not always the case and depends strongly on the values of  $d$ . If the values of the interaction matrix are small enough, then all equilibrium points are stable. A forthcoming paper will discuss a rigorous condition on the stability of equilibrium solutions with respect to  $d$ . All matrices  $d$  that have been used in this work provide only stable equilibrium points. This means that the stem cell will inevitably differentiate and assume one of the available cell states (equilibrium solutions). Supplementary Materials provides simple codes to verify the stability of the dynamical systems.

After studying the effects of weak inter-module interaction and external force fields separately, we can now focus on the case where both are present. The density plot of the quasi-potential is shown in Figure 5d. It is evident that there is an asymmetry along the  $\mathcal{M}$  coordinate, and the number of produced cells also differs. This approach can help in tuning the required number of produced cell types.

### 3.3. Random Hierarchical Branching

Given that we have no specific information about the system's parameter values, it would be more realistic to assume that these values are random variables. This section only considers parameter values that are given by

$$G_i = 2 + 0.1u_i, \quad (22)$$

$$\mu_i = 0.5u_i, \quad (23)$$

$$c_{ij} = 1.5(1 + u_i)\delta_{i,i-1}, \quad (24)$$

$$d_{ij} = 0.05u_i, \quad (25)$$

where  $u_i \sim U[-1, 1]$  and  $U[-1, 1]$  is the uniform distribution in  $[-1, 1]$ . Here,  $\delta$  represents the Kronecker delta. This scenario corresponds to a sequential branching.

The example shown in Figure 6 corresponds to a cell consisting of six hierarchically coupled and weakly interconnected gene modules under the influence of a random external field. Specifically, Figure 6a and 6b present the density and the 3D plot of the quasi-potential  $\Phi$ , respectively. All equilibrium points of this example are asymptotically stable (see Code6.m in Supplementary Materials). There are several noteworthy observations here that demonstrate the potential of this model to capture characteristics of the epigenetic landscape:

1. It is evident that there is highly complex branching of cell differentiation trajectories.
2. The produced cell states are highly stable (homeorhesis).
3. Some equilibrium states (cell states) are more probable than others.
4. Although the differentiation pathways are generally robust, it is possible for some trajectories to transition to another branch of cell state if the amount of random white noise is significantly increased. Even in this case, some transitions will be exceedingly rare as they belong to different dimensions. To make this possible, a series of  $m_i$ 's would have to transition simultaneously.
5. An alternative way of achieving state transitions is by returning the trajectory to a previous decision-making point (bifurcation). This is possible if the dynamic parameters  $r_i$  are significantly perturbed, a scenario that has not been analyzed in this work.
6. Some cell states are very rarely visited, and some others have not been visited at all during the limited number of simulation trajectories conducted in this work.
7. The above points are responsible for the rugged landscape of the generated quasi-potential.

Based on these observations, we can draw the following conclusions regarding the model's potential. First and foremost, points 1, 2, and 3 show that the model satisfies the three important conditions of Waddington's epigenetic landscape, i.e., (a) hierarchical branching, (b) homeorhesis, and (c) a specific cell-type ratio. Second, points 4 and 5 can model cell reprogramming. Specifically, the direct transition from one stable branch to another due to white noise (point 4) is related to direct reprogramming, also called

transdifferentiation. This type of reprogramming involves converting one mature somatic cell type into another mature somatic cell type without passing through a pluripotent stage [25]. Point 5 is related to indirect reprogramming, which requires the mature cell to revert back to a prior pluripotent or multipotent cell state before it can change its differentiation pathway and assume a new terminal cell state. This type of programming is also referred to as dedifferentiation. Point 6 demonstrates the ability of the model to describe cell states with a low probability of occurrence. Cancer cells are believed to correspond to this type of state within the epigenetic landscape, which preexists but is rarely assumed.

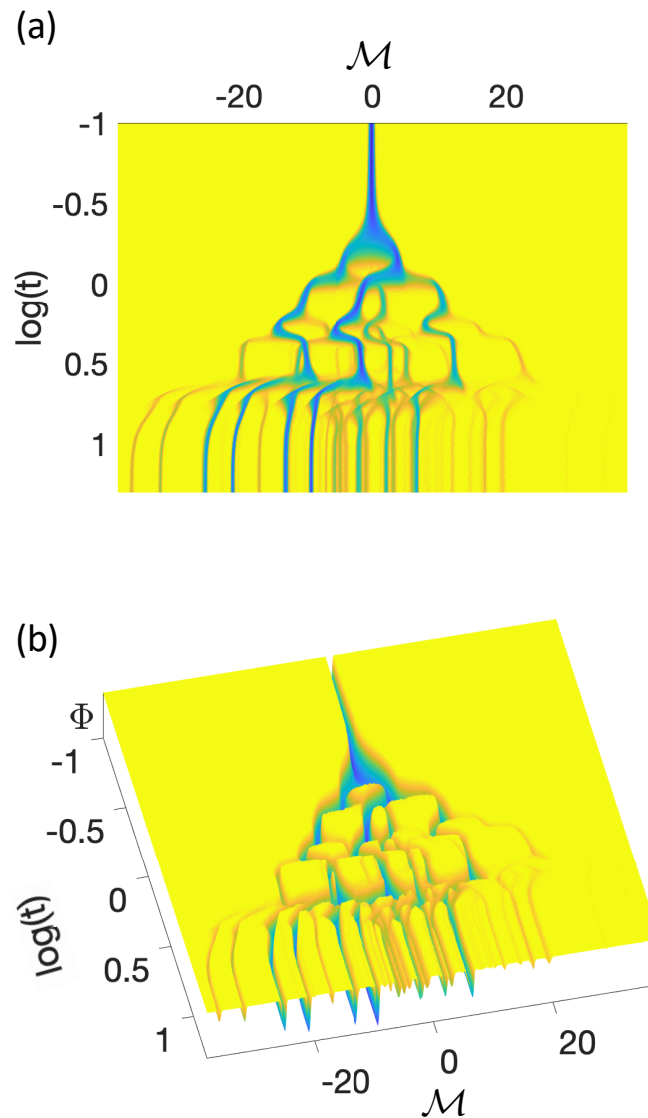


**Figure 6.** (a) Density plot and (b) 3D plot of the quasi-potential for  $n = 3$  and for random parameters determined by Equations (22)–(25). Blue and yellow correspond to low and high values of the quasi-potential, respectively.

#### 4. Conclusions

The purpose of the paper was to present a simple dynamical model that can capture three key features of Waddington's epigenetic landscape, namely hierarchical branching, homeorhesis, and precision in the number of produced cell types. The model was based on two hypotheses. The first hypothesis proposes that the GRN consists of gene modules that are hierarchically coupled. Initially, all modules are in an undecided state regarding

their function. Each module decides its function in a hierarchical manner, meaning that the first module makes a decision based on an external signal, which triggers the decision in the second module, and so on. Eventually, all modules perform a specific function, which collectively determines the type of the committed cell. The second hypothesis suggests that this process is regulated by external epigenetic factors.

Mathematically, each module was modeled as a dynamical system that exhibits a supercritical pitchfork or cusp bifurcation. For simplicity, this work implemented the normal form of these bifurcations. Additionally, each module was guided to the bifurcation point by regulating its parameters through a feedback mechanism originating from an external field representing epigenetic factors. Overall, the proposed complex system can describe self-organized hierarchical branching. Although the normal forms of one-dimensional bifurcations do not accurately capture the complexity of a real regulatory network, this work has demonstrated that such a simple dynamical system can phenomenologically describe the essential features of Waddington's epigenetic landscape.

In future studies, it would be interesting to apply this approach to more realistic RBNs. Specifically, it would be worthwhile to investigate a scenario where each module is modeled by a dynamical system exhibiting tristability [4]. In this case, as demonstrated in [8], the system exhibits Hopf bifurcation, and the generated cell states will be dynamic in nature. Furthermore, a more systematic study of the weakly coupled modules presented here may uncover more interesting attractors that are also dynamic in nature [9].

**Supplementary Materials:** The following supporting information can be downloaded at: <https://www.mdpi.com/article/10.3390/math12091380/s1>, Code S1: This code checks the stability of the dynamical system used in Figures 5d and 6.

**Funding:** This research received no external funding.

**Data Availability Statement:** The data presented in this study are available on request from the corresponding author.

**Conflicts of Interest:** The author declare no conflicts of interest.

## References

1. Kaern, M.; Elston, T.C.; Blake, W.J.; Collins, J.J. Stochasticity in gene expression: From theories to phenotypes. *Nat. Rev. Genet.* **2005**, *6*, 451–464. [[CrossRef](#)] [[PubMed](#)]
2. Raj, A.; van Oudenaarden, A. Nature, nurture, or chance: Stochastic gene expression and its consequences. *Cell* **2008**, *135*, 216–226. [[CrossRef](#)] [[PubMed](#)]
3. Waddington, C. *The Strategy of the Genes: A Discussion of Some Aspects of Theoretical Biology*; Allen & Unwin: London, UK, 1957.
4. Foster, D.V.; Foster, J.G.; Huang, S.; Kauffman, S.A. A model of sequential branching in hierarchical cell fate determination. *J. Theor. Biol.* **2009**, *260*, 589–597. [[CrossRef](#)] [[PubMed](#)]
5. Matsushita, Y.; Kaneko, K. Homeorhesis in Waddington's landscape by epigenetic feedback regulation. *Phys. Rev. Res.* **2020**, *2*, 023083. [[CrossRef](#)]
6. Huang, S. Reprogramming cell fates: Reconciling rarity with robustness. *BioEssays* **2009**, *31*, 546–560. [[CrossRef](#)] [[PubMed](#)]
7. Kang, C.; McElroy, M.; Voulgarakis, N.K. Emergent criticality in coupled Boolean networks. *Entropy* **2023**, *25*, 235. [[CrossRef](#)] [[PubMed](#)]
8. McElroy, M.; Green, K.; Voulgarakis, N.K. Self-regulated symmetry breaking model for Stem cell differentiation. *Entropy* **2023**, *25*, 815. [[CrossRef](#)]
9. Furusawa, C.; Kaneko, K. A dynamical-systems view of stem cell biology. *Science* **2012**, *338*, 215–217. [[CrossRef](#)]
10. MacArthur, B.D.; Lemischka, I.R. Statistical mechanics of pluripotency. *Cell* **2013**, *154*, 484–489. [[CrossRef](#)]
11. Garcia-Ojalvo, J.; Martinez Arias, A. Towards a statistical mechanics of cell fate decisions. *Curr. Opin. Genet. Dev.* **2012**, *22*, 619–626. [[CrossRef](#)]
12. Silva, J.; Smith, A. Capturing pluripotency. *Cell* **2008**, *132*, 532–536. [[CrossRef](#)] [[PubMed](#)]
13. Stanoev, A.; Schröter, C.; Koseska, A. Robustness and timing of cellular differentiation through population-based symmetry breaking. *Development* **2021**, *148*, dev197608. [[CrossRef](#)] [[PubMed](#)]
14. Hayashi, K.; Lopes, S.M.d.S.; Tang, F.; Surani, M.A. Dynamic equilibrium and heterogeneity of mouse pluripotent stem cells with distinct functional and epigenetic states. *Cell Stem Cell* **2008**, *3*, 391–401. [[CrossRef](#)]
15. Giuliani, A.; Tsuchiya, M.; Yoshikawa, K. Self-organization of genome Expression from embryo to terminal cell fate: Single-cell statistical mechanics of biological regulation. *Entropy* **2017**, *20*, 13. [[CrossRef](#)] [[PubMed](#)]
16. Ferrell, J.E. Bistability, bifurcations, and Waddington's epigenetic landscape. *Curr. Biol.* **2012**, *22*, R458. [[CrossRef](#)]

17. Naomi, M.; Cristina, P.; Arias, A.M. Transition states and cell fate decisions in epigenetic landscapes. *Nat. Rev. Genet.* **2016**, *17*, 693–703. [[CrossRef](#)]
18. Camacho-Aguilar, E.; Warmflash, A.; Rand, D.A. Quantifying cell transitions in *C. elegans* with data-fitted landscape models. *PLoS Comput. Biol.* **2021**, *17*, e1009034. [[CrossRef](#)]
19. Rand, D.A.; Raju, A.; Sáez, M.; Corson, F.; Siggia, E.D. Geometry of gene regulatory dynamics. *Proc. Natl. Acad. Sci. USA* **2021**, *118*, e2109729118. [[CrossRef](#)]
20. Karin, O.; Miska, E.A.; Simons, B.D. Epigenetic inheritance of gene silencing is maintained by a self-tuning mechanism based on resource competition. *Cell Syst.* **2023**, *14*, 24–40. [[CrossRef](#)]
21. Sáez, M.; Briscoe, J.; Rand, D.A. Dynamical landscapes of cell fate decisions. *Interface Focus* **2022**, *12*, 20220002. [[CrossRef](#)]
22. Sáez, M.; Blassberg, R.; Camacho-Aguilar, E.; Siggia, E.D.; Rand, D.A.; Briscoe, J. Statistically derived geometrical landscapes capture principles of decision-making dynamics during cell fate transitions. *Cell Syst.* **2022**, *13*, 12–28. [[CrossRef](#)] [[PubMed](#)]
23. Huang, S.; Ernberg, I.; Kauffman, S. Cancer attractors: A systems view of tumors from a gene network dynamics and developmental perspective. *Semin. Cell Dev. Biol.* **2009**, *20*, 869–876. [[CrossRef](#)] [[PubMed](#)]
24. MacArthur, B.D.; Ma, A.; Lemischka, I.R. Systems biology of stem cell fate and cellular reprogramming. *Nat. Rev.* **2009**, *10*, 672–681. [[CrossRef](#)] [[PubMed](#)]
25. Ng, N.; Newbery, M.; Maksud, S.; Dottori, M.; Sluyter, R.; Ooi, L. Transgene and chemical transdifferentiation of somatic cells for rapid and efficient neurological disease cell models. *Front. Cell. Neurosci.* **2022**, *16*, 858432. [[CrossRef](#)] [[PubMed](#)]
26. Hanna, J.; Saha, K.; Pando, B.; Van Zon, J.; Lengner, C.J.; Creyghton, M.P.; van Oudenaarden, A.; Jaenisch, R. Direct cell reprogramming is a stochastic process amenable to acceleration. *Nature* **2009**, *462*, 595–601. [[CrossRef](#)] [[PubMed](#)]
27. Zhou, J.X.; Aliyu, M.D.S.; Aurell, E.; Huang, S. Quasi-potential landscape in complex multi-stable systems. *J. R. Soc. Interface* **2012**, *9*, 3539–3553. [[CrossRef](#)] [[PubMed](#)]
28. Filipowicz, W.; Paszkowski, J. Gene silencing. In *Brenner's Encyclopedia of Genetics*, 2nd ed.; Academic Press: Cambridge, MA, USA, 2013; pp. 221–222. [[CrossRef](#)]
29. Di Santo, S.; Burioni, R.; Vezzani, A.; Muñoz, M.A. Self-Organized bistability associated with first-order phase transitions. *Phys. Rev. Lett.* **2016**, *116*, 240601. [[CrossRef](#)]
30. Strogatz, S.H. *Nonlinear Dynamics and Chaos: With Applications to Physics, Biology, Chemistry and Engineering*; Westview Press: Boulder, CO, USA, 2000.
31. Hartwell, L.H.; Hopfield, J.J.; Leibler, S.; Murray, A.W. From molecular to modular cell biology. *Nature* **1999**, *402*, C47–C52. [[CrossRef](#)] [[PubMed](#)]
32. Ihmels, J.; Friedlander, G.; Bergmann, S.; Sarig, O.; Ziv, Y.; Barkai, N. Revealing modular organization in the yeast transcriptional network. *Nat. Genet.* **2002**, *31*, 370–377. [[CrossRef](#)]
33. Ravasz, E.; Somera, A.L.; Mongru, D.A.; Oltvai, Z.N.; Barabási, A.L. Hierarchical organization of modularity in metabolic networks. *Science* **2002**, *297*, 1551–1555. [[CrossRef](#)]
34. Hernández, U.; Posadas-Vidales, L.; Espinosa-Soto, C. On the effects of the modularity of gene regulatory networks on phenotypic variability and its association with robustness. *Biosystems* **2022**, *212*, 104586. [[CrossRef](#)] [[PubMed](#)]
35. Hatleberg, W.L.; Hinman, V.F. Modularity and hierarchy in biological systems: Using gene regulatory networks to understand evolutionary change. *Curr. Top. Dev. Biol.* **2021**, *141*, 39–73. [[CrossRef](#)] [[PubMed](#)]

**Disclaimer/Publisher's Note:** The statements, opinions and data contained in all publications are solely those of the individual author(s) and contributor(s) and not of MDPI and/or the editor(s). MDPI and/or the editor(s) disclaim responsibility for any injury to people or property resulting from any ideas, methods, instructions or products referred to in the content.